Speckle variance detection of microvasculature using swept-source optical coherence tomography

Adrian Mariampillai,[1] Beau A. Standish,[1] Eduardo H. Moriyama,[1] Mamta Khurana,[1] Nigel R. Munce,[1] Michael K. K. Leung,[1] James Jiang,[5] Alex Cable,[5] Brian C. Wilson,[1] I. Alex Vitkin,[1,3,4] and Victor X. D. Yang[1,2,6,*]

[1]*Department of Medical Biophysics, University of Toronto, Toronto, M5G 2M9, Canada*
[2]*Department of Neurosurgery, University of Toronto, Toronto M5G 2M9, Canada*
[3]*Department of Radiation Oncology, University of Toronto, Toronto M5G 2M9, Canada*
[4]*Ontario Cancer Institute, Toronto M5G 2M9, Canada*
[5]*Thorlabs Inc., Newton, New Jersey 07860, USA*
[6]*Department of Electrical and Computer Engineering, Ryerson University, Toronto M5B 2K3, Canada*
[*]*Corresponding author: yangv@ee.ryerson.ca*

Received April 7, 2008; revised May 27, 2008; accepted May 30, 2008;
posted June 5, 2008 (Doc. ID 94708); published June 30, 2008

We report on imaging of microcirculation by calculating the speckle variance of optical coherence tomography (OCT) structural images acquired using a Fourier domain mode-locked swept-wavelength laser. The algorithm calculates interframe speckle variance in two-dimensional and three-dimensional OCT data sets and shows little dependence to the Doppler angle ranging from 75° to 90°. We demonstrate *in vivo* detection of blood flow in vessels as small as 25 μm in diameter in a dorsal skinfold window chamber model with direct comparison with intravital fluorescence confocal microscopy. This technique can visualize vessel-size-dependent vascular shutdown and transient vascular occlusion during Visudyne photodynamic therapy and may provide opportunities for studying therapeutic effects of antivascular treatments without on exogenous contrast agent. © 2008 Optical Society of America

OCIS codes: 110.4500, 170.3880, 170.4500, 170.5180, 170.2655.

Optical coherence tomography (OCT) [1] is a high-resolution (1–10 μm) modality used for minimally invasive imaging in anatomical sites, such as the retina, gastrointestinal tract, airways, and (coronary) vasculature [2]. Various OCT blood flow detection techniques [3–11] have been developed with velocity sensitivity ranging from 50–500 μm/s, depending on the minimum detectable frequency or phase shift and the Doppler angle. As microvasculature can be tortuous, the angular dependency of these techniques may lead to incomplete vascular maps *in vivo*. Fingler *et al.* [12] demonstrated a phase variance technique for detecting fluid mobility and transverse flow. Speckle variance techniques based on structural image intensity have been used in tumor microvascular imaging with high-frequency ultrasound [13,14]. Spectral speckle analysis has also been attempted in OCT [15]. However, its performance is hindered by the computational complexity and slow frame rate in the initial demonstration. Recent developments in swept-wavelength lasers [16] and the application of Fourier domain mode locking (FDML) [17] can provide an imaging frame rate up to 370 kHz, which may yield a sufficient imaging speed for real-time microvascular imaging using speckle-based techniques.

In this Letter we report a simple and computationally efficient microvascular detection algorithm based on interframe speckle variance processing of structural image intensity using an FDML swept-source optical coherence tomography (SS-OCT) system and demonstrate its performance in a flow phantom and an animal model. As shown in Fig. 1, the SS-OCT system uses a 43–67 kHz FDML fiber-ring laser source incorporating a polygon-based tunable filter [7] with a sweeping range of 112 nm centered at 1310 nm, −6 dB ranging depth of 6 mm in air (corresponding to a coherence length of 12 mm), axial resolution of ~8 μm in tissue, and average output power of 48 mW. The total cavity length used in FDML the laser ranges from 3.3 to 4.5 km. A fiber Bragg grating provides the A-scan trigger and OCT signal recalibration was performed as previously described in [18]. Interframe speckle variance images (SV_{ijk}) of the structural OCT intensity (I_{ijk}) are calculated across $N=3$ B-mode images as

$$SV_{ijk} = \frac{1}{N}\sum_{i=1}^{N} (I_{ijk} - I_{\mathrm{mean}})^2,$$

where j and k are lateral and depth indices of the B-mode images and i denotes the B-mode slice index with I_{mean} as the average over the same set of pixels.

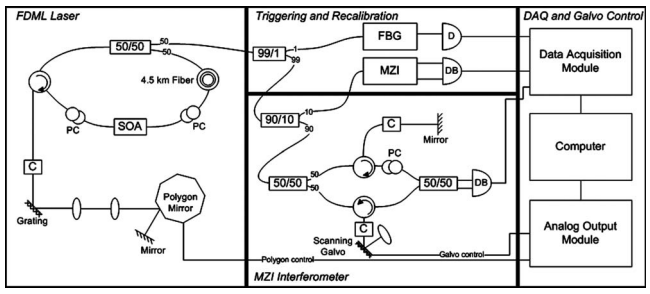

Fig. 1. Schematic of the FDML SS-OCT system. SOA, semiconductor optical amplifier; PC, polarization controller; C, collimator; FBG, fiber Bragg grating; MZI, Mach–Zehnder interferometer; D, detector; DB, dual balanced detector.

A flow phantom study was performed to evaluate the relationship among speckle variance, flow velocity, and the Doppler angle. Figure 2 shows Doppler and speckle variance images of a 600 μm inner diameter polymer tube filled with 0.5% Intralipid driven by a syringe pump. The tube was embedded in Agarose gel mixed with Intralipid such that the fluid and gel had similar scattering properties. SS-OCT images (2000 $\times$512 pixels) were acquired at four different Doppler angles (75°, 80°, 85°, and 89.5°) with the pump off or on (24 mm/s peak velocity, assuming laminar flow). Doppler images were processed using phase-based color Doppler signal processing techniques [6] with an ensemble length of 16 A-scans. For speckle variance imaging, four adjacent A-scans were averaged together to improve the signal-to-noise ratio of the structural image [5,15], leading to a decrease in the speckle variance noise floor. Figure 2 demonstates that the speckle variance has little dependence on the Doppler angle or flow velocity and can even distinguish the Intralipid fluid from the surrounding gel at a zero bulk flow rate.

We directly compared speckle variance imaging with intravital fluorescence confocal microscopy using a dorsal skinfold window chamber model (WCM) in athymic nude mice (NCRNU-M, Taconic) [19] as shown in Figs. 3a and 3b, where the exposed skin flap and cutaneous microvasculature were protected by a glass coverslip window. Surgery, confocal microscopy, and SS-OCT imaging were carried out under ketamine–xylazine anesthesia with the mice maintained at body temperature. All procedures were carried out with institutional approval at the Princess Margaret Hospital, Toronto, Canada. Fluorescence confocal imaging (LSM 510 Meta NLO, Zeiss, excitation 488 nm, collection 530$\pm$15 nm bandpass) was performed using 5 mg kg^{-1} of 500 kD fluorescein labeled dextran via tail vein injection. A 5$\times$ (NA =0.25) objective was used for imaging a 1.8 mm $\times$1.8 mm region of the window from which a z stack of ten images was acquired within 10 min of tail vein injection, each having a 40 μm depth of focus and step size of 20 μm between images. Three-dimensional (3D) (1000$\times$2000$\times$512 pixels) speckle variance OCT was performed in the same region; total imaging time of the 3D volume was approximately 1 min (limited by data acquisition and transfer). For both the confocal and OCT image stacks,

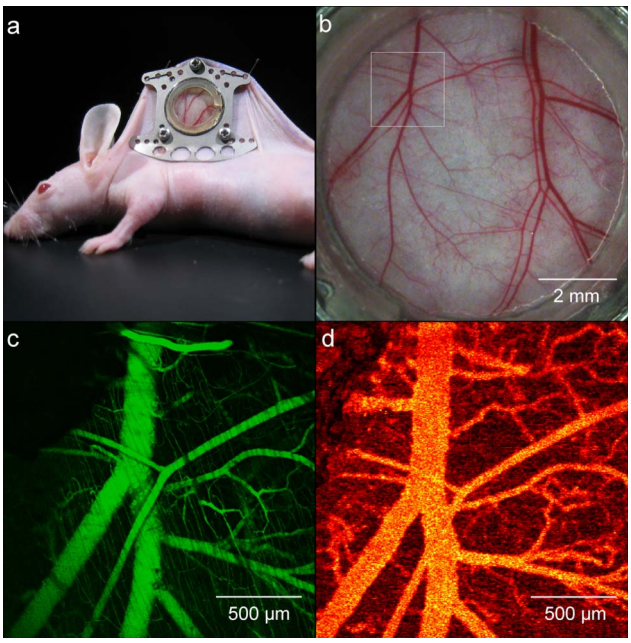

Fig. 3. (Color online) a, Dorsal skinfold WCM. b, White light microscopy of entire window. The white box represents the approximate location of confocal and OCT imaging. c, Maximum intensity projection image of a fluorescence confocal z stack obtained using 500 kD fluorescein labeled dextran (1.8$\times$1.8 mm). d, Speckle variance OCT *en face* projection image of vasculature without the use of any external contrast agents (1.8 mm$\times$1.8 mm).

maximum intensity projection was performed in the depth direction to obtain *en face* vascular maps as shown in Figs. 3c and 3d, respectively. The smallest vessels detectable by speckle variance imaging were ~25 μm in diameter. The capillary bed, consisting of microvessels ~5 μm in diameter as detected by the fluorescence confocal microscopy, was below the lateral resolution of the OCT system (15 μm).

Speckle variance OCT imaging can be used to monitor antivascular treatment effects dynamically. In Fig. 4, we demonstrate detection of microvascular changes induced by Visudyne photodynamic therapy (PDT) by imaging before, during, and immediately posttreatment. The PDT treatment parameters were Visudyne 2 mg/kg, light exposure 10 min at 690 nm, with a fluence rate of ~42 mW/cm^2. Rapid shutdown of the smaller blood vessels within the treatment region was observed approximately 1 min after light

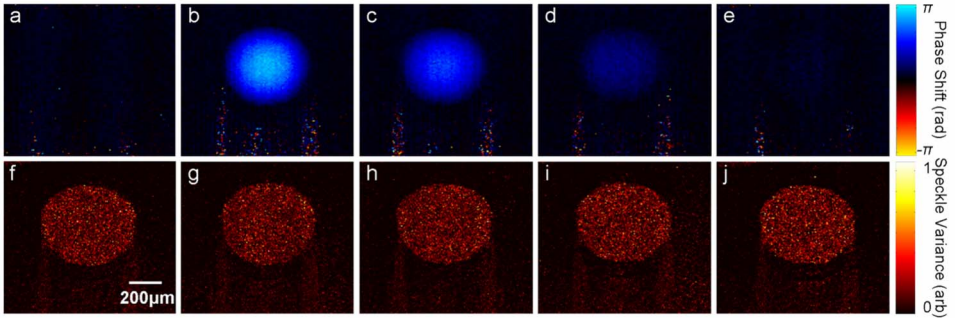

Fig. 2. (Color online) a, Doppler phase shift measured for stationary Intralipid within a 600 μm tube at an 80° Doppler angle. b–e, Doppler phase shift measured from Intralipid moving through the tube at a rate of 12 ml/h for Doppler angles of 75°, 80°, 85°, 89.5°, respectively. f–g, Corresponding normalized (to fixed value for all images) speckle variance images.

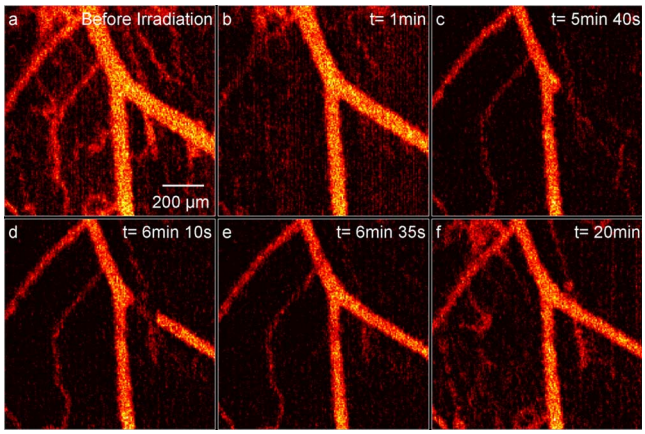

Fig. 4. (Color online) Speckle variance OCT imaging of Visudyne-mediated PDT within a 1 mm × 1 mm region of the dorsal skinfold window chamber mouse model (fluence rate = 42 mW/cm^2, total fluence = 25 J/cm^2, treatment time = 10 min). a, Vasculature prior to laser irradiation. b, One minute after start of laser irradiation. c, Total shutdown of right branch. d, Reperfusion of right branch with imaging artifact. e, Reperfusion of right branch without imaging artifact. f, 10 min postend of laser irradiation showing reperfusion, but main vessels still appear to be constricted.

exposure began (Fig. 4b, $t = 1$ min). A transient localized total occlusion of one of the larger vessels occurred between $t = 5$ min 40 s and 6 min 35 s, with a partial reperfusion event at 6 min 27 s (Figs. 4c–4e). At the end of the PDT light irradiation (Fig. 4f), there was persistent vascular shutdown of the smaller vessels, and the larger vessels had an approximately 30% reduction of diameter as measured by speckle variance OCT.

The main advantage of the speckle variance processing technique compared with conventional Doppler OCT is its simplicity, since it can be implemented in real time to provide additional Doppler angle-independent microvascular information with little additional computational complexity. Being based on intrinsic contrast, this technique also has a potential benefit over fluorescence microscopy, especially when imaging leaky neovasculature, where background saturation can occur rapidly owing to abnormal vessel permeability and extravascation of fluorescent markers. Like phase-variance-based techniques [12], speckle variance detection also suffers from multiple scattering induced artifacts leading to artificial speckle variance contrast beneath the blood vessels. Another key disadvantage is the effect of interframe bulk tissue motion, which can dominate the speckle variance. However, higher-frame-rate (>1000 fps) FDML OCT systems are being developed for volumetric imaging that may remove artifacts owing to physiological motion. At these very high frame rates, speckle decorrelation between frames may not be complete, thus leading to a decrease in speckle variance contrast. However, it may also be possible to quantitatively relate the amount of decorrelation to the flow velocity within the vessel. For such systems, interframe speckle variance may be an attractive technique to detect, quantify, and monitor effects of vascular targeted therapies, such as PDT and antivascular drugs in animal models beyond the geometric confines of the WCM.

In summary, we have shown interframe speckle variance detection of microcirculation using an FDML polygon-based SS-OCT system in a flow phantom and compared its imaging performance with intravital fluorescence confocal microscopy techniques in an *in vivo* WCM. We demonstrated that speckle variance OCT could detect vessel size dependent vascular shutdown and transient vessel occlusion during PDT.

This research was supported by the Natural Sciences and Engineering Research Council of Canada, the Canadian Foundation for Innovation, and the Canadian Institutes of Health Research.

References

1. D. Huang, E. A. Swanson, C. P. Lin, J. S. Schuman, W. G. Stinson, W. Chang, M. R. Hee, T. Flotte, K. Gregory, C. A. Puliafito, and J. G. Fujimoto, Science **254**, 1178 (1991).
2. M. E. Brezinski, *Optical Coherence Tomography: Principles and Applications* (Academic, 2006).
3. Z. Ding, Y. Zhao, H. Ren, J. Nelson, and Z. Chen, Opt. Express **10**, 236 (2002).
4. V. Westphal, S. Yazdanfar, A. M. Rollins, and J. A. Izatt, Opt. Lett. **27**, 34 (2002).
5. V. Yang, M. Gordon, B. Qi, J. Pekar, S. Lo, E. Seng-Yue, A. Mok, B. Wilson, and I. Vitkin, Opt. Express **11**, 794 (2003).
6. B. White, M. Pierce, N. Nassif, B. Cense, B. Park, G. Tearney, B. Bouma, T. Chen, and J. de Boer, Opt. Express **11**, 3490 (2003).
7. B. Vakoc, S. Yun, J. de Boer, G. Tearney, and B. Bouma, Opt. Express **13**, 5483 (2005).
8. R. K. Wang, Phys. Med. Biol. **52**, N531 (2007).
9. A. H. Bachmann, M. L. Villiger, C. Blatter, T. Lasser, and R. A. Leitgeb, Opt. Express **15**, 408 (2007).
10. S. Makita, Y. Hong, M. Yamanari, T. Yatagai, and Y. Yasuno, Opt. Express **14**, 7821 (2006).
11. V. X. D. Yang and I. A. Vitkin, in *Handbook of Optical Coherence Tomography in Cardiology* (Marcel Dekker, 2006).
12. J. Fingler, D. Schwartz, C. Yang, and S. E. Fraser, Opt. Express **15**, 12636 (2007).
13. V. X. D. Yang, A. Needles, D. Vray, S. Lo, B. C. Wilson, and S. Foster, Proc.-IEEE Ultrason. Symp. **1**, 453 (2004).
14. A. M. Cheung, A. S. Brown, V. Cucevic, M. Roy, A. Needles, V. X. D. Yang, D. J. Hicklin, R. S. Kerbel, and F. S. Foster, Ultrasound Med. Biol. **33**, 1259 (2007).
15. J. K. Barton and S. Stromski, Opt. Express **13**, 5234 (2005).
16. W. Y. Oh, S. H. Yun, G. J. Tearney, and B. E. Bouma, Opt. Lett. **30**, 3159 (2005).
17. R. Huber, D. C. Adler, and J. G. Fujimoto, Opt. Lett. **31**, 2975 (2006).
18. R. Huber, M. Wojtkowski, J. G. Fujimoto, J. Y. Jiang, and A. E. Cable, Opt. Express **13**, 10523 (2005).
19. G. H. Algire and F. Y. Legallais, J. Natl. Cancer Inst. (1940–1978) **10**, 225 (1949).